Available online at www.sciencedirect.com

ScienceDirect

www.elsevier.com/locate/jes

JES JOURNAL OF ENVIRONMENTAL SCIENCES

www.jesc.ac.cn

Efficient degradation of drug ibuprofen through catalytic activation of peroxymonosulfate by Fe_3C embedded on carbon

*Guangli Zhang, Yaobin Ding, Wenshan Nie, Heqing Tang**

College of Resources and Environmental Science, South-Central University for Nationalities, Wuhan 430074, China

ARTICLE INFO

Article history:
Received 9 March 2018
Revised 14 September 2018
Accepted 8 October 2018
Available online 13 October 2018

Keywords:
Catalytic degradation
Ibuprofen
Iron carbide
N-doped carbon
Peroxymonosulfate

ABSTRACT

Ibuprofen (IBU), a nonsteroidal anti-inflammatory drug, is becoming an important member of pharmaceuticals and personal care products (PPCPs) as emerging pollutants. To degrade IBU, magnetic Fe_3C nanoparticles embedded on N-doped carbon (Fe_3C/NC) were prepared as a catalyst by a sol–gel combustion method. As characterized, the Fe_3C/NC nanoparticles were composed of a NC nano-sheet and capsulated Fe_3C particles on the sheet. The Fe_3C/NC nanoparticles were confirmed an efficient catalyst for peroxymonosulfate (PMS) activation to generate sulfate radicals ($SO_4^{\bullet-}$), single oxygen ($^1O_2$) and hydroxyl radicals (•OH) toward the degradation of IBU. The added IBU (10 mg/L) was almost completely removed in 30 min by using 0.1 g/L Fe_3C/NC and 2 g/L PMS. The catalyst was confirmed to have good ability and excellent reusability through leaching measurements and cycle experiments. A catalytic mechanism was proposed for the catalytic activation of PMS on Fe_3C/NC, which involves both Fe_3C reactive sites and N-doped carbon matrix as reactive sites in Fe_3C/NC. Moreover, the degradation pathway of IBU in the Fe_3C/NC-PMS system was proposed according to the detections of degradation intermediates.

Introduction

Ibuprofen (IBU), as a medication in the nonsteroidal anti-inflammatory drug class, is widely used in the treatment of toothache, headache, back pain, muscle soreness, rheumatoid arthritis and cold fever (Hersh et al., 2000; Madhavan et al., 2010; Musa and Eriksson, 2007; Wilson, 1999). Its bioaccumulation poses a risk to human health and to the safety and balance of ecosystems, and it is shown that long-term intake of trace levels of IBU can cause biological deformities and microbial resistance (Vieno et al., 2005). Therefore, new methods for efficient removing IBU are urgently needed. Advanced oxidation processes (AOPs) are techniques that activate green oxidants by introducing external energy or a catalyst and utilize the free radicals produced during the activation process to degrade and mineralize organic contaminants (Glaze et al., 1987). Sulfate radical ($SO_4^{\bullet-}$, oxidation–reduction potential (E^0) = 2.5–3.1 V) based oxidation processes are becoming a new class of AOPs, and the generation of $SO_4^{\bullet-}$ may be achieved by activation of peroxymonosulfate (PMS).

* *Corresponding author. E-mail:* tangheqing@mail.scuec.edu.cn. (Heqing Tang).

https://doi.org/10.1016/j.jes.2018.10.002
1001-0742 © 2018 The Research Center for Eco-Environmental Sciences, Chinese Academy of Sciences. Published by Elsevier B.V.

The most efficient catalyst for the activation of PMS has been demonstrated to be Co-based catalysts (Anipsitakis and Dionysiou, 2003, 2004). However, cobalt leaching is a barrier to its practical application. Heterogeneous Fe-based catalysts are an alternative to Co-based catalysts due to their environment-friendly natures (Ding et al., 2016, 2013; Rastogi et al., 2009). The reported heterogeneous Fe-based catalysts have some obvious shortcomings. For example, their chemical stability is not so good during the PMS activation; their catalytic ability requires to be promoted by further introducing external energies (Avetta et al., 2014; Cai et al., 2015; Zhang et al., 2012); and they may meet catalyst poisoning problem (Zhang et al., 2013). Therefore, it is urgently needed to develop more efficient and stable heterogeneous Fe-based catalysts.

Recently, we are developing Fe-containing and/or carbon-based materials as a bifunctional material having both strong adsorptive ability and excellent catalytic ability (Ding et al., 2017; Qin et al., 2016). During the fabrication of Fe-containing carbon-based materials, we found the existence of iron carbide and observed the positive effect of iron carbide on the related catalytic processes. Although the catalytic activity of Fe-based oxides have been extensively studied (An et al., 2013; Ding et al., 2013; Ren et al., 2017; Wang et al., 2010; Xuan et al., 2009; Yu et al., 2016), the catalysis of iron carbide is rarely reported. This stimulated us to develop an iron carbide catalyst here. Iron carbide often exists as a special phase in iron and iron alloys, where iron carbide phase is highly stable (Dodelet et al., 2014; Hu et al., 2015, 2014). Hu et al. (2014) fabricated Fe_3C-containing composite as an electro-catalysts by using a high-pressure pyrolysis method. Niu et al. (2016) investigated the electrocatalysis of oxygen reduction reaction on a Fe_3C-containing composite. Kraupner et al. (2010) used mesoporous Fe_3C sponges as magnetic supports and as heterogeneous catalyst for ammonia decomposition, which yielded the conversion of ammonia more than 95% at 700°C. However, to the best of our knowledge, the use of Fe_3C-containing composite has not been reported for AOPs, especially for the catalytic activation of PMS to degrade organic pollutants.

In the present work, we prepared Fe_3C nanoparticles on NC as an efficient and stable catalyst of PMS activation for the degradation of IBU. We intended to prepare single-Fe_3C nanoparticles, but we could not eliminate the residual carbon in the produced catalyst. Therefore, we prepared Fe_3C nanoparticles on NC instead. The use of NC (N-doped carbon) as the second component was also rising from several considerations. Mesoporous carbon is a good adsorptive substrate, being benefit to the followed catalytic decomposition of adsorbed IBU. We have confirmed recently that N-doped graphene shows excellent catalytic activity in the activation of persulfate for the degradation of bisphenol A (Wang et al., 2015a), and N-doped carbon materials have been also reported to be highly efficient electrocatalysts for oxygen reduction reaction (Gong et al., 2009; Guo et al., 2016; Zhao et al., 2013). As anticipated, the developed Fe_3C/NC composites showed good chemical stability, excellent reusability, and high catalytic activity for the activation of PMS. The use of 0.1 g/L Fe_3C/NC in the presence of 2.0 g/L PMS could achieve a complete degradation of the added IBU.

1. Materials and methods

1.1. Chemicals

$Fe_3Cl{\cdot}6H_2O$ (purity 99.9%), hexadecyltrimethylammonium bromide (CTAB), ethanol (99.7%), melamine (99.8%) and zero-valence iron (ZVI) powders were obtained from Sinopharm Chemical Reagent Co., Ltd. (Shanghai, China). PMS ($2KHSO_5{\cdot}$-$KHSO_4{\cdot}K_2SO_4$, 4.7% active oxygen) was purchased from Shanghai D&R Finechem Co., Ltd. (Shanghai, China). IBU were purchased from Sigma–Aldrich. All chemicals were used as received without further purification. Deionized water was used in the present work.

1.2. Preparation of Fe_3C/NC

Fe_3C/NC was prepared according to a previous report (Wang et al., 2015b). Typically, 2.52 g melamine and 2.7 g $Fe_3Cl{\cdot}6H_2O$ were added into 80 mL of ethanol–water (1:1, V/V) mixture. Under stirring, CTAB (2.92 g) was then added until the mixture was stirred evenly. The obtained clear solution was transferred to a water bath and heated at 80°C for 4 hr, which was accompanied by continuous agitation. Then, the solution-containing beaker was moved into an oven and heated to dry the solution at 100°C for 12 hr, resulting in the generation of a khaki solid. The whole process was carried out in an air atmosphere without nitrogen protection. The dried powder was transferred to a quartz tube furnace to anneal at 680°C for 3 hr under a nitrogen flow of 160 mL/min and the final product was denoted as Fe_3C/NC.

1.3. Characterization

Powder X-ray diffraction (XRD) patterns of the catalyst were recorded on Bruker Advanced D8 X-ray diffractometer with Cu $K\alpha$ radiation (D8 ADVANCE, Bruker, Germany), operated at 40 mA and 40 kV. The morphology was investigated by scanning electron microscopy (SEM, SU8010, Hitachi, Japan) with an acceleration voltage of 50 kV and transmission electron microscopy (TEM, Tecnai G220 S-TWIN, FEI, USA) with an acceleration voltage of 200 kV. The valence change of elements in the catalysts before and after reaction was characterized by a MULT1LAB 2000 X-ray photoelectron spectrometer (XPS) from Thermo Fisher with a monochromatic Al $K\alpha$ X-ray source (MULTILAB2000, Thermo Scientific, USA). All binding energies were corrected to the C 1 s peak (284.6 eV). Brunauere–Emmette–Teller (BET) measurement was carried out on an Autosorb-iQ analyzer (Autosorb-iQ, Quantachrome Instruments, USA). Thermogravimetric analysis (TGA) was carried out with a Netzsch TG209 F3 thermal analyzer (TG209 F3, Netzsch, Germany).

1.4. Catalytic experiments

The catalytic oxidative decomposition of IBU was carried out at 30°C. Fe_3C/NC (0.1 g/L) was well dispersed in 50 mL of 10 mg/L IBU solution with a pre-adjustment of pH by using NaOH and HCl. After a pre-adsorption of 30 min for achieving adsorption/desorption equilibrium, PMS with

specified amounts was added to the reaction solution. At given time intervals, 1 mL of the reaction solution was sampled, followed by a rapid addition of excess pure ethanol (0.05 mL) to quench the reaction and then a centrifugation to remove the solid particles for further analysis. The concentration of IBU in solution was determined by high performance liquid chromatography (HPLC, UltiMate 3000 series, Thermo Scientific, USA). All the experiments were repeated three times, and the results were reproducible within the experimental errors (±5%). The data were discussed by using their averaged values.

1.5. Chemical analysis

The concentrations of IBU were analyzed by a HPLC system (UltiMate 3000 series, Thermo Scientific, USA) with an ultraviolet (UV) detector at a wavelength of 220 nm. The separation column was an amethyst C18-P column (5 μm, 4.6 mm × 150 mm). The mobile phase used for HPLC was a mixture of acetonitrile and 0.6% acetic acid (60:40, V/V), which was filtered through 0.2 μm filter prior to use. The flow rate was set at 1.0 mL/min and the injection volume was 20 μL. The degradation intermediates of IBU in the Fe_3C/NC-PMS system were identified by liquid chormatography-mass spectrometry (LC–MS, 1100 LC/MSD Trap, Agilent, USA) and gas chromatography–mass spectrometry (GC–MS, TRACE 1300, Thermo Fisher, USA).

2. Results and discussion

2.1. Characterization of Fe_3C/NC

As observed from the SEM image in Fig. 1a, Fe_3C/NC exhibited a sheet-like structure with irregular wrinkles and the sheet-like structures were packed to produce fairly large pores. The TEM observation in Fig. 1b indicated that black Fe_3C nanoparticles (NPs) with sizes of about 42 nm were embedded in a folded sheet-like carbon. The high resolution transmission electron microscopy (HRTEM) image of Fe_3C/NC (Fig. 1c) further illustrated that the Fe_3C NP was surrounded by a thin crystalline shell with a thickness of about 2 nm. As discussed later, a calculation from the XRD data indicated that the particle size of Fe_3C NPs was about 37 nm. Therefore, the thin crystalline shell with a thickness of about 2 nm might be carbon materials.

Fig. 1d gives the N_2 adsorption/desorption isothermal and pore size distribution diagram (inset in Fig. 1d). Fe_3C/NC exhibited IV isotherm with H3 hysteresis loop and possessed a specific surface area of 127 m^2/g with well-distributed pore size of 38.2 nm, indicating that the Fe_3C/NC nanocomposites were mesoporous. Meanwhile, the BET specific surface area of NC, Fe_3O_4 and Fe_2O_3 as control was measured as 1972, 63 and 9 m^2/g, respectively (Appendix A Table S1).

Fig. 1e shows the XRD patterns of Fe_3C/NC, which matched well with the Fe_3C standard diffraction card (Jade PDF#76–1877) and were completely out of line with other iron species such as Fe and Fe_2C. The diffraction peaks at 2θ 37.8, 42.8, 43.9, 45.0, 45.8 and 49.2° were assigned to the (021), (121), (210), (103), (211) and (113) crystalline planes of Fe_3C, respectively. The average grain size of the Fe_3C particles (D) was calculated to be 36.8 nm, according to the Scherrer's formula (Eq. (1)):

$$D = K\lambda/\beta\cos\theta \quad (1)$$

where, K is the Scherrer constant, λ is the X-ray wavelength, β is the peak width at half maximum height and θ is the Bragg diffraction angle. The second component NC was not observable in the XRD pattern of the Fe_3C/NC composite.

The formation of graphitic carbon in the pyrolysis process was clearly demonstrated by the Raman spectrum of Fe_3C/NC (Fig. 1f). In the spectrum, the G-band for graphitic carbon appeared at about 1580 cm^{-1}, and the D-band for amorphous carbon located at about 1350 cm^{-1}. The D-band is related to the disordered arrangement of graphite atoms or defects, curl and charge traps in the edges of graphene, the G peak is due to the vibration of sp^2 carbon atoms in the plane (Stankovich et al., 2007). I_D/I_G is the ratio of the integrated intensities of the D and G bands, which reveals the degree of graphitization of samples (Wang et al., 2014; Xu et al., 2011). As observed from Fig. 1f, the intensity ratio of the D- to G-band (I_D/I_G) for Fe_3C/NC was 0.82. The low ratio of integrated intensity of the D to G band (I_D/I_G) indicated the formation of ordered graphitized structures due to increase in average size of the sp^2 domains upon the generation of on the carbon matrix.

Fig. 1g shows the TG profile of the composite in air at a heating rate of 10°C/min to the final temperature of 950°C. The weight loss between 200 and 450°C was attributed to the removal and destruction of functional groups adsorbed on the carbon surface, and the marked weight loss in the range from 450 to 550°C was ascribed to the combustion of the NC support into CO_2 and nitrogen oxides gas. When the temperature reached 550°C, the weight of the composite remained unchanged. We inferred that Fe_3C was finally decomposed into Fe_2O_3 at the high temperatures. The Fe_3C content (x) can be calculated by Eq. (2):

$$x = 2/3 \times (m_2/m_1) \times (M_{Fe_3C}/M_{Fe_2O_3}) \times 100\% \quad (2)$$

where, m_1 is the mass of Fe_3C/NC, M_{Fe3C} is the formula mass of Fe_3C, and m_2 and M_{Fe2O3} are the residual mass and formula mass of Fe_2O_3, respectively. The content of Fe_3C was evaluated as 41.1 wt.%.

2.2. IBU degradation by using Fe_3C/NC as a catalyst

The catalytic degradation of IBU was conducted by using Fe_3C/NC as a catalyst in the presence of PMS. As shown in Fig. 2, in the control experiment, the addition of PMS (2 g/L) in the absence of any catalyst brought about IBU removal of only 3.0% after 30 min, revealing that IBU degradation could not be induced directly by PMS. Similarly, the addition of Fe_3C/NC in the absence of PMS removed little IBU by considering a light adsorption of IBU on Fe_3C/NC. However, when Fe_3C/NC and PMS were simultaneously added, the added IBU was almost completely degraded

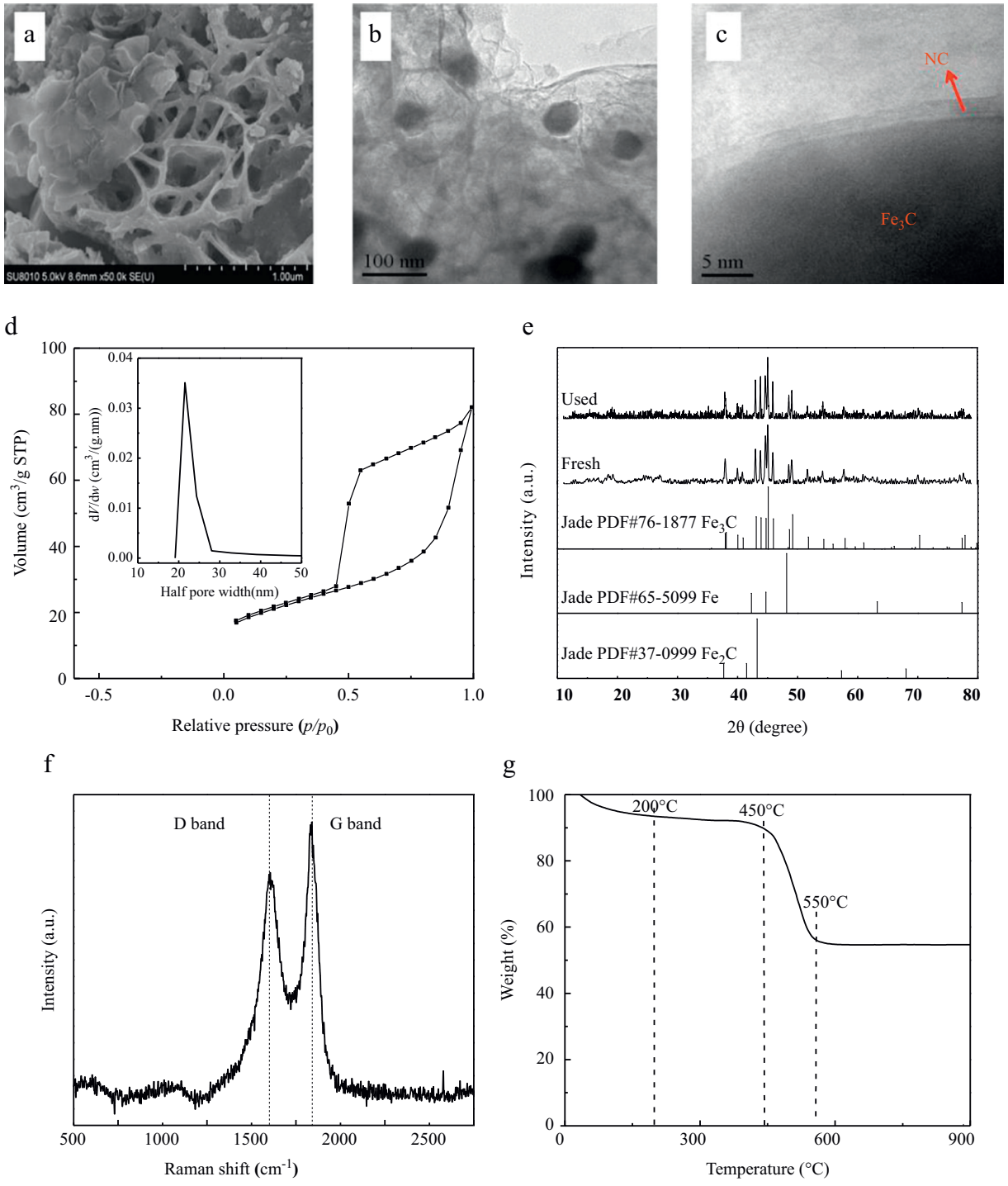

Fig. 1 – (a) Scanning electron microscopy (SEM) image, (b) transmission electron microscopy (TEM) image, (c) high resolution TEM (HRTEM) image, (d) N_2 adsorption–adsorption curve (the inset showing the pore size distributions), (e) X-ray diffraction (XRD) pattern, (f) Raman spectrum, and (g) thermogravimetric analysis (TGA) curve of magnetic Fe_3C nanoparticles embedded on N-doped carbon (Fe_3C/NC).

after 30 min. This clearly demonstrated Fe_3C/NC was an efficient catalyst of the PMS activation for the degradation of IBU. As a comparison, the use of NC and ZVI powders induced 40% and 39.8% removal of IBU in 30 min, respectively, while Fe_3O_4 and Fe_2O_3 NPs showed no obvious catalytic activity for the activation of PMS and degradation of IBU.

In the tested systems, the IBU degradation followed a pseudo-first-order kinetic model (Eq. (3)):

$$\ln(C_t/C_0) = -kt \quad (3)$$

where, t (min) is the reaction time, k (min^{-1}) is the apparent rate constant, and C_0 and C_t are IBU concentrations at time t =

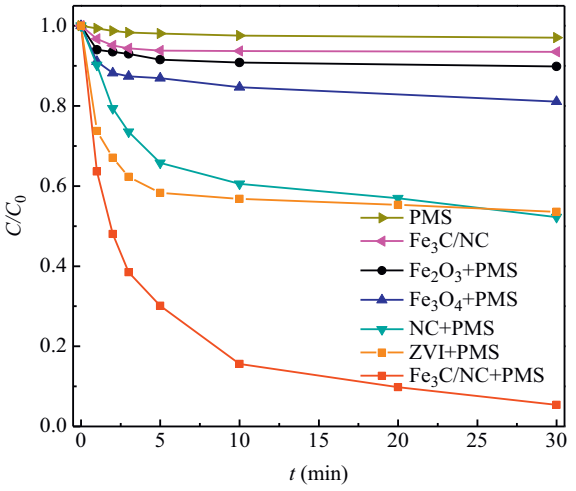

Fig. 2 – Ibuprofen (IBU) degradation in different systems at 30°C. Reaction conditions: initial IBU concentration 10 mg/L, catalyst load 0.1 g/L, and initial peroxymonosulfate (PMS) concentration 2.0 g/L. C_0 and C: IBU concentrations at time t = 0 and t, respectively; t: the reaction time; ZVI: zero-valent iron.

0 and t, respectively. By data fitting, it was obtained that the k-value for Fe_3C/NC was 0.34 min^{-1}, being 3.1 times that for NC (0.11 min^{-1}). Considering the much higher BET specific surface area of NC (1972 m^2/g) than Fe_3C/NC (127 m^2/g), we normalized the obtained rate constant by dividing the obtained k value with specific surface area of the catalyst (load 0.1 g/L). The normalized apparent rate constant was referred to as k_{SSA}. As calculated, the k_{SSA} value for Fe_3C/NC (0.54 $m^{-2}\cdot min^{-1}$) was 28.42 times that for NC (0.019 $m^{-2}\cdot min^{-1}$), indicating that Fe_3C/NC had much higher catalytic activity than NC and that Fe_3C in Fe_3C/NC was the main reactive sites for the catalytic degradation of IBU.

The IBU degradation was investigated under various conditions as shown in Fig. 3. As catalyst load was increased from 0 to 0.1 g/L, the k value was increased significantly from 0.0059 to 0.34 min^{-1} (Fig. 3a). By further increasing the load to 0.2 g/L, the k-value was slightly decreased to 0.30 min^{-1}. This can be accounted for by that greater catalyst load yielded more catalytic active sites, inducing the generation of more reactive radicals and then faster and more efficient degradation of IBU. However, the addition of excess catalyst generated excess reactive radicals, and caused self-quenching of the reactive radicals rather than pollutant degradation.

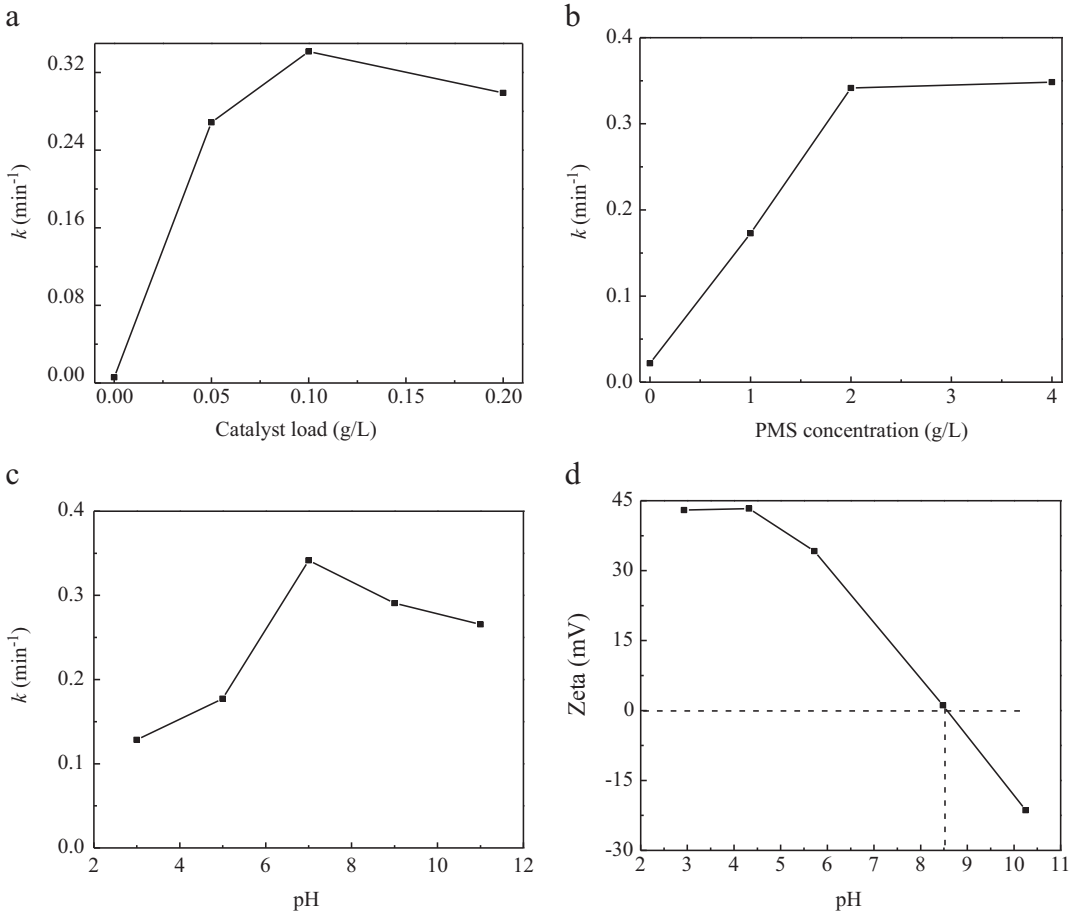

Fig. 3 – Effects of (a) catalyst load, (b) PMS concentration, and (c) pH on the degradation rate constant of IBU (k). (d) Zeta potentials of Fe_3C/NC.

The effect of PMS concentration on IBU degradation was investigated in Fig. 3b. A general trend was observed that the *k*-value was increased with increasing PMS concentration. When the PMS concentration was increased from 0 to 1, 2 and 4 g/L, the *k* value was significantly increased from 0.022 to 0.17, 0.34 and 0.35 min^{-1} correspondingly. This was mainly because the increased PMS concentration allowed more reactive radicals being produced by the catalysis of Fe_3C/NC. It should be noted that once $SO_4^{\bullet-}$ is generated by Fe_3C/NC-induced catalytic activation of PMS, $SO_4^{\bullet-}$ may react with HSO_5^- to produce $SO_5^{\bullet-}$ according to Eq. (4):

$$HSO_5^- + SO_4^{\bullet-} \rightarrow SO_5^{\bullet-} + HSO_4^- \quad (4)$$

This consumes the generated $SO_4^{\bullet-}$, but the secondly generated $SO_5^{\bullet-}$ is usually considered as being not responsible for the degradation of organic pollutants when adding excessive amounts of PMS (Anipsitakis and Dionysiou, 2003). In the present work, 2 g/L was selected as optimal PMS concentration.

Fig. 3c shows the effect of pH on the catalytic activity of Fe_3C/NC. As the initial solution pH was increased from 3 to 11, the degradation rate constant of IBU was first increased and then decreased after passing a maximum at pH ≈ 8. The activation under acidic conditions produced too many $SO_4^{\bullet-}$ radicals, which enhanced radical-radical scavenger reactions, being unfavorable the degradation of IBU. Under alkaline conditions, OH^- reacted with $SO_4^{\bullet-}$ to produce SO_4^{2-} according to Eq. (5):

$$SO_4^{\bullet-} + OH^- \rightarrow SO_4^{2-} + \bullet OH \quad (5)$$

Because the longevity of $SO_4^{\bullet-}$ (half-life time 4 sec) is longer than that of •OH (half-life time less than 1 μsec (Banerjee and Konar, 1984), this reaction was unbeneficial to the contact with pollutants and then the degradation of organic pollutants. The measured zeta potentials of Fe_3C/NC (Fig. 5d) indicated that the surface of the catalyst was negatively charged at pH > 8.5. PMS mainly existed in the form of SO_4^{2-} and HSO_5^- at pH = 8.5–11. Because of the electrostatic repulsion between PMS and the negatively charged surface of the catalyst, it was difficult for PMS to adsorb on the catalyst surface, which is detrimental to activate PMS to produce active radicals for IBU degradation. The observed effects of pH on the IBU degradation are similar to that obtained in the studies of heterogeneous Co-based catalysts for the PMS activation to degrade organic pollutants (Chen et al., 2008; Shi et al., 2012). Under neutral conditions, Co-based catalysts exhibit good heterogeneous catalytic properties.

2.3. Stability and reusability of Fe_3C/NC

In order to investigate the reusability of Fe_3C/NC, at the end of each run of the degradation experiment, the catalyst was recollected with a magnet, washed several times with deionized water, and then dispersed in 50 mL of 10 mg/L IBU solution, and then a next run of the degradation experiment. These steps were repeated several cycles. It was found that the recycled Fe_3C/NC kept good catalytic activity, achieving a IBU degradation removal of 91% or more (at 30 min) for the successive six cycles (Fig. 4). This confirmed the good stability of Fe_3C/NC during the catalytic degradation of IBU. After the six runs of the degradation experiment, the Fe_3C/NC was recollected by vacuum filtration and dried. The crystal structure of the recollected catalyst was characterized by XRD (Fig. 1e). It was found that the XRD patterns of the used catalyst were almost the same as that of the fresh catalyst.

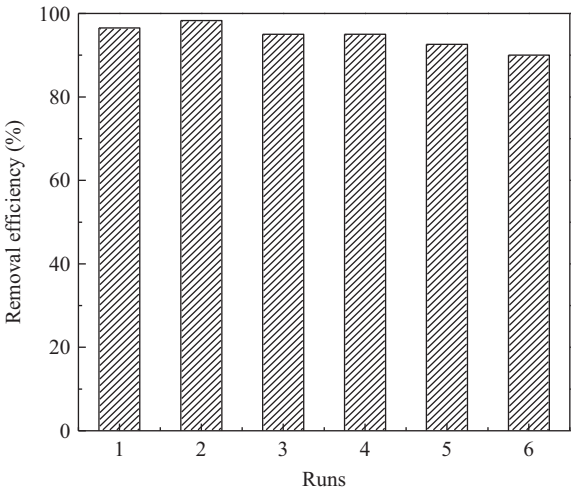

Fig. 4 – IBU degradation in different runs. Reaction conditions: initial IBU concentration 10 mg/L, catalyst load 0.1 g/L, and initial PMS concentration 2.0 g/L.

To evaluate the stability of Fe_3C/NC, Fe leaching was monitored during the IBU degradation with the addition of 0.1 g/L Fe_3C/NC (total Fe content was 0.038 g/L). The atomic absorption spectroscopy analysis indicated that the Fe leaching was 0.119 mg/L after the reaction lasted for 120 min, accounting for 0.3% of the total Fe content. Therefore, Fe_3C/NC has good chemical stability during the reaction.

2.4. Mechanism for the catalytic activation of PMS by Fe_3C/NC

The mechanism of the activation of PMS on metal- and carbon-based catalysts have been studied, and it is generally believed that catalysts are used as electron donors, resulting in •OH, $SO_4^{\bullet-}$ and $SO_5^{\bullet-}$ being produced according to Eqs. (6)–(9) during the activation of PMS by heterogeneous catalysts (Duan et al., 2015a, 2015b):

$$HSO_5^- + e^- \rightarrow \bullet OH + SO_4^{2-} \quad (6)$$

$$HSO_5^- + e^- \rightarrow \bullet OH + SO_4^{\bullet-} \quad (7)$$

$$HSO_5^- + e^- \rightarrow H^+ + SO_5^{\bullet-} \quad (8)$$

$$SO_4^{\bullet-} + OH^- \rightarrow \bullet OH + SO_4^{2-} \quad (9)$$

In the present work, the generated dominant radical species were identified by radical quenching experiments

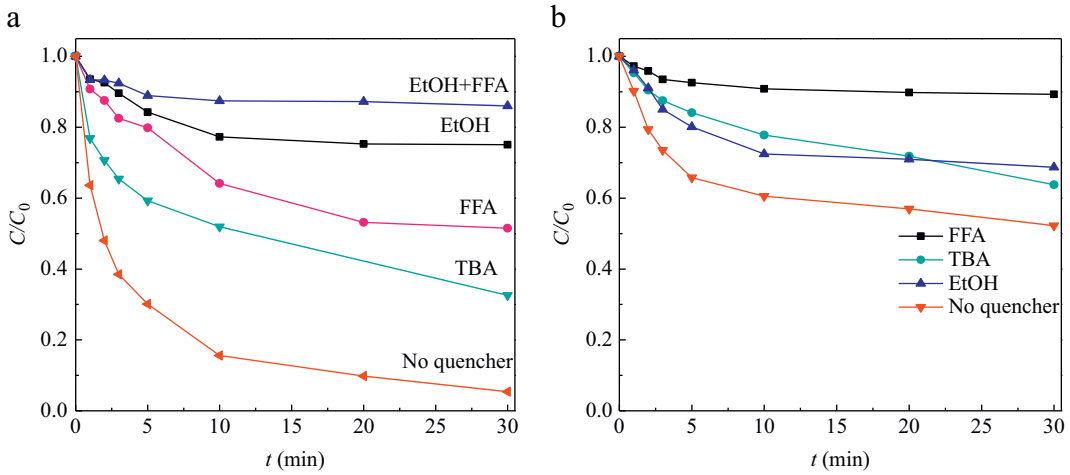

Fig. 5 – Effects of radical quenchers on the degradation of IBU (10 mg/L) in the presence of 2.0 g/L PMS and the catalyst of (a) 0.1 g/L Fe_3C/NC and (b) 0.059 g/L NC. EtOH: ethanol; FFA: furfuryl alcohol; TBA: *tert*-butanol.

(Fig. 5). The amount of 0.059 g/L NC was equal to that of NC in 0.1 g/L Fe_3C/NC according to the TGA results. The addition of the quencher was 100 times that of PMS in molar ratio. The reaction rate constants of *tert*-butanol (TBA) with •OH is 3.8×10^8–7.6×10^8 L/(mol·sec), being 418–1900 times greater than that of TBA with $SO_4^{\bullet-}$ which is 4×10^5–9.1×10^5 L/(mol·sec) (Rastogi et al., 2009). Thus, TBA was used as a quencher for •OH in the IBU degradation system. The reaction rate constants of ethanol (EtOH) with •OH and $SO_4^{\bullet-}$ were 1.6×10^7–7.7×10^7 L/(mol·sec) and 1.2×10^9–2.8×10^9 L/(mol·sec) (Ding et al., 2013), respectively. The two rate constants are equivalent, so that ethanol was used as a quencher of •OH and $SO_4^{\bullet-}$. When the alcohol capturing agent was not added, the degradation rate of IBU was 95.0% within 30 min. After the addition of EtOH, the removal of IBU was decreased to only 24.9%. The addition of EtOH inhibited the removal of IBU. After adding TBA, the removal of IBU was 67.4%. The much more decrease of the degradation efficiency by EtOH than by TBA suggested that •OH and $SO_4^{\bullet-}$ coexisted during the activation of PMS by Fe_3C/NC. However, ethanol cannot completely quench the reaction. In view of recent reports (Liang et al., 2017; Nie et al., 2017; Zhou et al., 2015), PMS can be activated by benzoquinone, carbonaceous materials and metallic oxides to produce single oxygen ($^1O_2$). Therefore, furfuryl alcohol (FFA), which can rapidly be degraded by the attack of $^1O_2$, was selected as a probe. As shown in Fig. 5a, the presence of FFA decreased the degradation efficiency from 95.0% to 48.5% in Fe_3C/NC–PMS system, suggesting that $^1O_2$ was also responsible for Fe_3C/NC–PMS–IBU system. When adding EtOH and FFA, the pollutant degradation removal was decreased significantly to 14.0%. Therefore, the degradation of IBU in Fe_3C/NC–PMS system was attributed a combination of free radicals and non-free radical, and their contribution ratio was estimated to be 3:2 by rough calculations. As shown in Fig. 5b, the addition of EtOH and TBA had little influence on the degradation efficiency in NC–PMS–IBU system, while the presence of FFA obviously inhibited the degradation of IBU. The result indicated that $^1O_2$ was the main reactive species involved in the degradation of IBU in NC–PMS system. Therefore, it was concluded that •OH and $SO_4^{\bullet-}$ were mainly produced through the activation of PMS by Fe_3C reactive sites, while the generation of $^1O_2$ in Fe_3C/NC–PMS system was mainly attributed to the activation of PMS by NC in Fe_3C/NC.

XPS analysis was carried out to clarify the change of the valence and content of the surface elements of Fe_3C/NC and estimate the possible catalytic mechanism. As shown in Fig. 6a, the surface composition of Fe_3C/NC before and after the reaction was almost the same. The Fe 2p envelop was consistent with that reported previously (Cappus et al., 1995; Lu et al., 2007). For the high-resolution Fe 2p spectrum of the fresh catalyst (Fig. 6b), it was deconvoluted into three peaks at 711.3, 725.0 and 719.0 eV, being assigned to the Fe $2p_{3/2}$, Fe $2p_{1/2}$ and shake-up satellite of Fe^{3+}, respectively. After the degradation operation, the observed Fe $2p_{3/2}$ and Fe $2p_{1/2}$ peaks could be further deconvoluted into two peaks be attributing to Fe^{2+} and Fe^{3+}, respectively. The high-resolution XPS Fe 2p spectrum of the used catalyst indicated that the content of Fe^{2+} was increased to 32%, which was accompanied by the weakening of the Fe^{3+} signal. This demonstrated that part of Fe^{3+} was transformed to Fe^{2+}, and there was a Fe^{2+}/Fe^{3+} cycling on the catalyst surface during the degradation experiment.

The peaks for the fresh catalyst appear at 284.5, 285.7 and 288.1 eV, which are attributed to C=C/C–C, C–OH and C=O groups. The content of C=C/C–C at 284.5 eV took up 77% for the fresh catalysts, indicating that the most of C was present in the form of cross-linked cellular lattices (Fig. 6c). The C–OH bonding configurations become enhanced after the degradation experiment, which indicates the catalyst surface was hydroxylated during the reaction. Moreover, C=O groups was generated due to the oxidation of C=C/C–C.

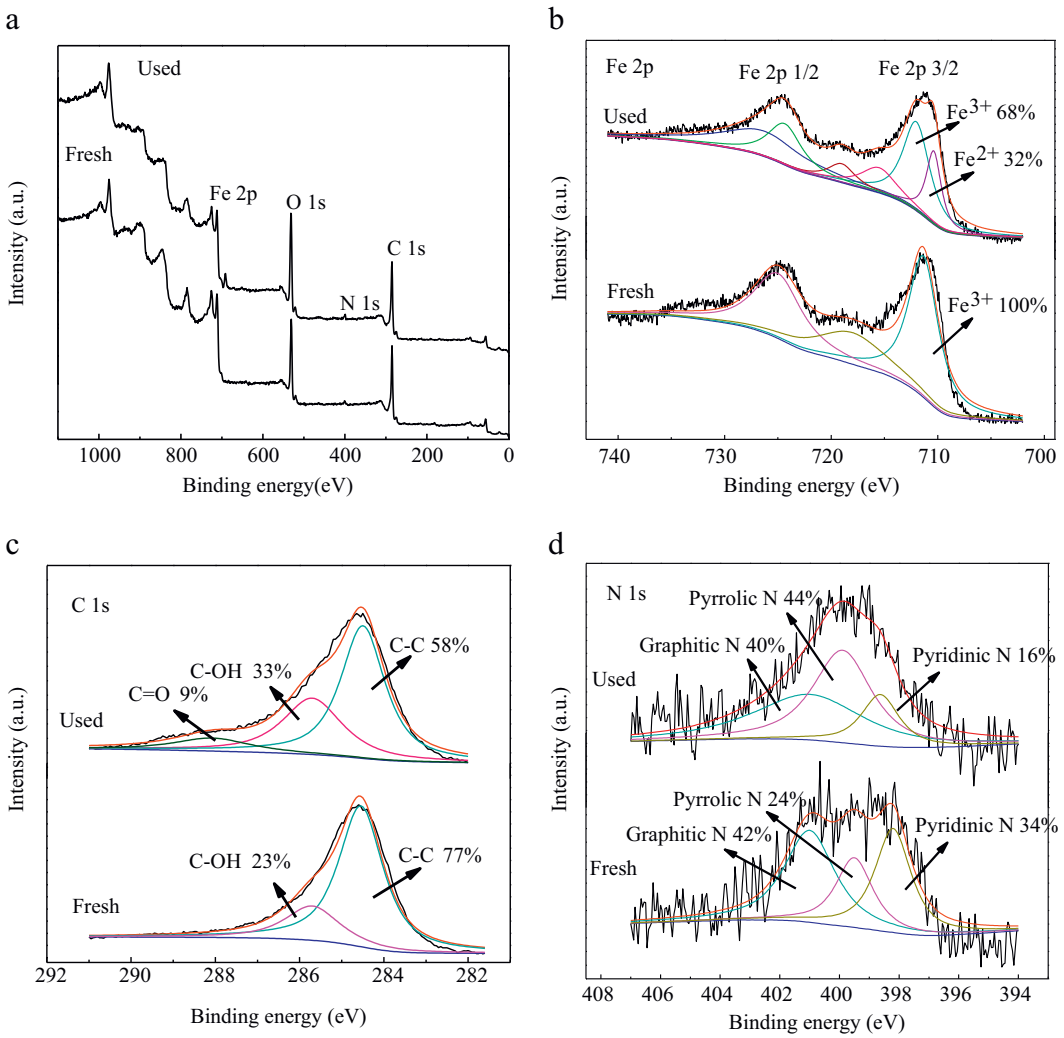

Fig. 6 – X-ray photoelectron spectroscopy (XPS) spectra of Fe_3C/NC before and after the degradation experiment: (a) wide scan survey, (b) Fe 2p, (c) C 1 s, and (d) N 1 s envelops.

The catalytic ability of carbon materials may be enhanced by N-doping (Wang et al., 2015a). Guo et al. (2016) clarified active sites of N-doped carbon materials for oxygen reduction reaction using model catalysts and found the ORR active site is created by pyridinic N. In the present work, pyridinic N (398.2 eV), pyrrolic N (399.5 eV), and graphitic N (401.0 eV) were identified from the XPS spectrum of the fresh catalyst in the N 1 s core level (Fig. 6d). After being used, the content of pyridinic N was decreased from 34% to 16%, revealing that the doped N in Fe_3C/NC played a key role in PMS activation. The binding energies slightly shifted to higher binding energy values after the degradation experiment, which inferred that there was an electron transfer between PMS and nitrogen groups through a possible coordination. Similar positive shift of binding energy value of N 1s orbit was reported by Yao et al. (2017). Considering that pyridinic N creates Lewis base sites that reduce the energy barrier of the reactants adsorbed on adjacent carbon atoms and accelerates the first electron transfer, we believe that NC in our work can enhance the number of active sites and the generation of $^1O_2$.

According to the above results and discussion, a mechanism for the enhanced activation of PMS by Fe_3C/NC was proposed in Fig. 7, which may be expressed by Eqs. (10)–(13).

$$HSO_5^- + Fe^{3+} \rightarrow SO_5^{\bullet-} + Fe^{2+} + H_2O \quad (10)$$

$$HSO_5^- + Fe^{2+} \rightarrow SO_4^{\bullet-} + Fe^{3+} + OH^- \quad (11)$$

$$SO_4^{\bullet-} + H_2O \rightarrow \bullet OH + H^+ + SO_4^{2-} \quad (12)$$

$$HSO_5^- + SO_5^{2-} \xrightarrow{NC} HSO_4^- + SO_4^{2-} + {}^1O_2 \quad (13)$$

Firstly, IBU in solution is adsorbed on the Fe_3C/NC surface by π–π interaction between the support NC and carbon shell with IBU molecular. As shown in Fig. 2, about

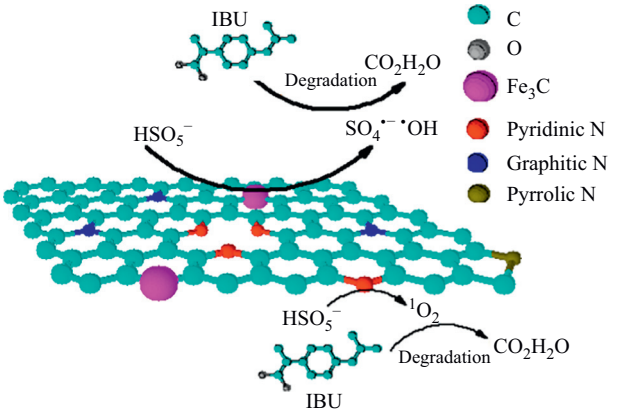

Fig. 7 – Possible reaction mechanism of IBU degradation in the system of Fe_3C/NC–PMS.

6.5% IBU can be removed in 30 min by the adsorption effect of Fe_3C/NC. The Fe_3C domains function as active sites for electron transport to activate PMS according to Eqs. (10)–(12). Once PMS is added, $SO_5^{\bullet-}$ is generated from PMS being activated by the unveiled activation sites including Fe^{3+}. Then the generated Fe^{2+} sites catalyzed the decomposition of PMS to $SO_4^{\bullet-}$. A portion of $SO_4^{\bullet-}$ reacts with H_2O to form •OH. The generated $SO_4^{\bullet-}$ and •OH reacted with IBU, leading to the degradation of IBU. Secondly, the presence of the support NC and carbon shell enhanced electron transfer process due to their excellent electronic conductivity, which is like the role of noble metals in PMS activation (Ahn et al., 2016). As a result, PMS activation can be fastened. Meanwhile, the N-doped carbon area also acts as active sites to transfer electron and generate $^1O_2$ (Eq. (13)) from PMS activation. Therefore, Fe_3C/NC can be used as a stable and efficient environmental catalyst in the degradation of pollutants through the synergistic effect between Fe_3C and NC.

2.5. *Reaction pathways of IBU degradation*

To analyze the degradation intermediates of IBU in the Fe_3C/NC–PMS system, the reaction solution sampled in degradation time of 10 min was analyzed by liquid chormatography–mass spectrometry (LC–MS) (Appendix A Fig. S1) and gas chromatography–mass spectrometry (GC–MS) (Appendix A Fig. S2). Through LC–MS analysis, compounds 1–6 were identified, while compounds 1 and 7–11 were detected by GC–MS analysis. The molecular ion masses and MS2 (the secondary mass spectrometry) fragmentation patterns for the main intermediates were given in Appendix A Fig. S1. Compound 1 was identified as IBU with *m/z* (mass charge ratio) 207 and two fragments at *m/z* 181 and 161. As a primary intermediate, compound 2 with *m/z* 221 and one fragment at *m/z*

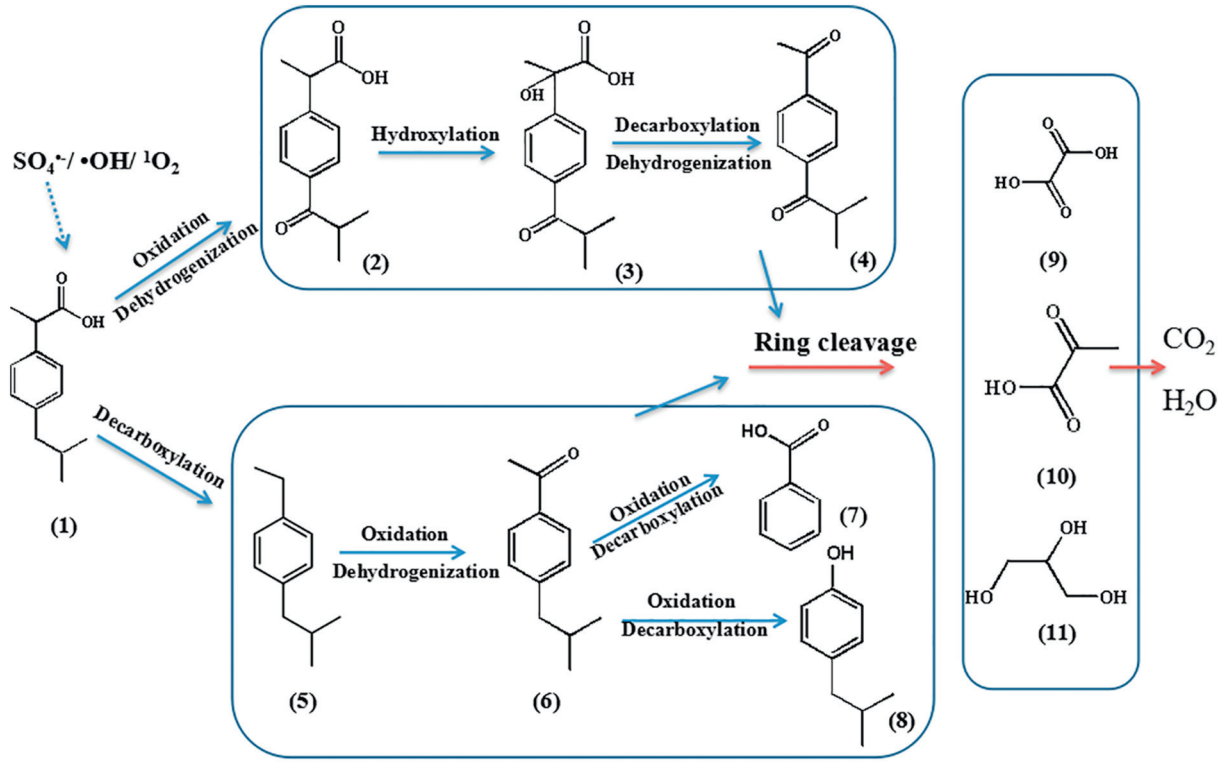

Fig. 8 – Proposed reaction pathways of IBU degradation in the Fe_3C/NC–PMS system. $^1O_2$: single oxygen.

175 was identified as 2-(4-isobutyrylphenyl)propanoic acid. The same intermediate was also reported previously for the photocatalytic degradation of IBU (Choina et al., 2013). Then, the degradation processes of IBU in the Fe_3C/NC–PMS and Fe_3C/NC–PMS–EtOH systems were investigated by HPLC (Appendix A Fig. S3). When the alcohol capturing agent was not added, the peaks at 2.1, 4.5, 5.4 and 8.0 min in the HPLC diagram were compounds 2, 3, 1 and 5, respectively. After the addition of EtOH, there were four peaks at 1.5, 5.4, 8.0 and 8.7 min corresponding to compounds 4, 1, 5 and 6. A possible mechanism was the attack of isobutyl substituents on the side chain of IBU by generated hydroxyl radicals or sulfate radicals in the study. On the other hand, the attack of propionic acid on the side chain of IBU by generated radicals and nonradicals produced another primary intermediate compound 5 with *m/z* 163 and five fragments at *m/z* 144, 120, 105, 91 and 57. Decarboxylation reaction was suggested as a main degradation pathway for IBU in the systems of oxone-MnO_x/silica and photo-Fenton (Mendez-Arriaga et al., 2010; Yang et al., 2017). Compound 3 was formed through the addition of a hydroxyl group on the carbon side chain of the compound 2, and then was further transformed to compound 4 through decarboxylation and dehydrogenation. Meanwhile, compound 5 underwent hydroxylation and dehydrogenation to form compound 6, which was further oxidized to compounds 7 or 8. As ring cleavage of intermediates, three compounds 9–11 were identified by GC–MS (Appendix A Fig. S2). Based on the above mentioned results, the oxidative degradation pathway of IBU mainly by hydroxyl radicals or sulfate radicals in the system of Fe_3C/NC–PMS was proposed in Fig. 8.

3. Conclusions

Magnetic Fe_3C/NC composites were successfully synthesized through a pyrolysis method. It was found that Fe_3C/NC had a superior catalytic activity for the activation of PMS toward the degradation of IBU. The good catalytic performances were attributed to the functions of Fe(III) and N-doped carbon matrix in Fe_3C/NC. The quenching experiments confirmed the generation of $SO_4^{\bullet-}$, •OH and $^1O_2$ as the major reactive species for the degradation of IBU. •OH and $SO_4^{\bullet-}$ were mainly produced through the activation of PMS by Fe_3C reactive sites, while the generation of $^1O_2$ in Fe_3C/NC-PMS system was mainly attributed to the activation of PMS by NC in Fe_3C/NC. Based on the LC–MS and GC–MS analysis of the degradation intermediates, the pathways for IBU degradation were proposed. The mineralization process of IBU involved the steps of oxidation, carboxylation/decarboxylation, dehydration, dehydrogenization and ring cleavage. The high-efficiency and good stability of the catalyst support that the catalyst has significant potentials for the application in the field of pollution control.

Acknowledgements

This work was supported by the National Natural Science Foundation of China (Nos. 21777194 and 21507168).

Appendix A. Supplementary data

Supplementary data to this article can be found online at https://doi.org/10.1016/j.jes.2018.10.002.

REFERENCES

Ahn, Y.Y., Yun, E.T., Seo, J.W., Lee, C.H., Kim, S.H., Kim, J.H., et al., 2016. Activation of peroxymonosulfate by surface-loaded noble metal nanoparticles for oxidative degradation of organic compounds. Environ. Sci. Technol. 50, 10187–10197.

An, J.J., Zhu, L.H., Wang, N., Song, Z., Yang, Z.Y., Du, D.Y., et al., 2013. Photo-Fenton like degradation of tetrabromobisphenol a with graphene $BiFeO_3$ composite as a catalyst. Chem. Eng. J. 219, 225–237.

Anipsitakis, G.P., Dionysiou, D.D., 2003. Degradation of organic contaminants in water with sulfate radicals generated by the conjunction of peroxymonosulfate with cobalt. Environ. Sci. Technol. 37, 4790–4797.

Anipsitakis, G.P., Dionysiou, D.D., 2004. Radical generation by the interaction of transition metals with common oxidants. Environ. Sci. Technol. 38, 3705–3712.

Avetta, P., Pensato, A., Minella, M., Malandrino, M., Maurino, V., Minero, C., et al., 2014. Activation of persulfate by irradiated magnetite: implications for the degradation of phenol under heterogeneous photo-fenton-like conditions. Environ. Sci. Technol. 49, 1043–1050.

Banerjee, M., Konar, R.S., 1984. Comment on the paper "polymerization of acrylonitrile initiated by $K_2S_2O_8$-Fe(II) redox system". Polym. Chem. Ed. 22, 1193–1195.

Cai, C., Zhang, H., Zhong, X., Hou, L.W., 2015. Ultrasound enhanced heterogeneous activation of peroxymonosulfate by a bimetallic Fe-Co/SBA-15 catalyst for the degradation of Orange II in water. J. Hazard. Mater. 283, 70–79.

Cappus, D., Haßel, M., Neuhaus, E., Heber, M., Rohr, F., Freund, H.J., 1995. Polar surfaces of oxides: reactivity and reconstruction. Surf. Sci. 337, 268–277.

Chen, X.Y., Chen, J.W., Qiao, X.L., Wang, D.G., Cai, X.Y., 2008. Performance of nano-Co_3O_4/peroxymonosulfate system: kinetics and mechanism study using Acid Orange 7 as a model compound. Appl. Catal. B 80, 116–121.

Choina, J., Kosslick, H., Fischer, C., Flechsig, G.U., Frunza, L., Schulz, A., 2013. Photocatalytic decomposition of pharmaceutical ibuprofen pollutions in water over titania catalyst. Appl. Catal. B 129, 589–598.

Ding, Y.B., Zhu, L.H., Wang, N., Tang, H.Q., 2013. Sulfate radicals induced degradation of tetrabromobisphenol a with nanoscaled magnetic $CuFe_2O_4$ as a heterogeneous catalyst of peroxymonosulfate. Appl. Catal. B 129, 153–162.

Ding, Y.B., Tang, H.B., Zhang, S.H., Wang, S.B., Tang, H.Q., 2016. Efficient degradation of carbamazepine by easily recyclable microscaled $CuFeO_2$ mediated heterogeneous activation of peroxymonosulfate. J. Hazard. Mater. 317, 686–694.

Ding, Y.B., Ruan, Y.F., Zhu, L.H., Tang, H.Q., 2017. Efficient oxidative degradation of chlorophenols by using magnetic surface carboxylated Cu^0/Fe_3O_4 nanocomposites in a wide pH range. J. Environ. Chem. Eng. 5, 2681–2690.

Dodelet, J.P., Chenitz, R., Yang, L., Lefèvre, M., 2014. A new catalytic site for the electroreduction of oxygen. ChemCatChem 6, 1866–1867.

Duan, X.G., Sun, H.Q., Kang, J., Wang, Y.X., Indrawirawan, S., Wang, S.B., 2015a. Insights into heterogeneous catalysis of persulfate activation on dimensional-structured nanocarbons. ACS Catal. 5, 4629–4636.

Duan, X.G., O'Donnell, K., Sun, H.Q., Wang, Y.X., Wang, S.B., 2015b. Sulfur and nitrogen co-doped graphene for metal-free catalytic oxidation reactions. Small 11, 3036–3044.

Glaze, W.H., Kang, J.W., Chapin, D.H., 1987. The chemistry of water treatment processes involving ozone, hydrogen peroxide and ultraviolet radiation. Ozone Sci. Eng. 9, 335–352.

Gong, K.P., Du, F., Xia, Z.H., Durstock, M., Dai, L.M., 2009. Nitrogen-doped carbon nanotube arrays with high electrocatalytic activity for oxygen reduction. Science 323, 760–764.

Guo, D., Shibuya, R., Akiba, C., Saji, S., Kondo, T., Nakamura, J., 2016. Active sites of nitrogen-doped carbon materials for oxygen reduction reaction clarified using model catalysts. Science 351, 361–365.

Hersh, E.V., Moore, P.A., Ross, G.L., 2000. Over-the-counter analgesics and antipyretics: a critical assessment. Clin. Ther. 22, 500–548.

Hu, Y., Jensen, J.O., Zhang, W., Cleemann, L.N., Xing, W., Bjerrum, N.J., et al., 2014. Hollow spheres of iron carbide nanoparticles encased in graphitic layers as oxygen reduction catalysts. Angew. Chem. Int. Ed. 53, 3675–3679.

Hu, Y., Jensen, J.O., Zhang, W., Martin, S., Chenitz, R., Pan, C., et al., 2015. Fe_3C-based oxygen reduction catalysts: synthesis, hollow spherical structures and applications in fuel cells. J. Mater. Chem. A 3, 1752–1760.

Kraupner, A., Antonietti, M., Palkovits, R., Schlicht, K., Giordano, C., 2010. Mesoporous Fe_3C sponges as magnetic supports and as heterogeneous catalyst. J. Mater. Chem. 20, 6019–6022.

Liang, P., Zhang, C., Duan, X.G., Sun, H.Q., Liu, S.M., Tade, M.O., et al., 2017. An insight into metal organic framework derived N-doped graphene for the oxidative degradation of persistent contaminants: formation mechanism and generation of singlet oxygen from peroxymonosulfate. Environ. Sci: Nano. 4, 315–324.

Lu, L.R., Ai, Z.H., Li, J.P., Zheng, Z., Li, Q., Zhang, L.Z., 2007. Synthesis and characterization of Fe-Fe_2O_3 core-shell nanowires and nanonecklaces. Cryst. Growth Des. 7, 459–464.

Madhavan, J., Grieser, F., Ashokkumar, M., 2010. Combined advanced oxidation processes for the synergistic degradation of ibuprofen in aqueous environments. J. Hazard. Mater. 178, 202–208.

Mendez-Arriaga, F., Esplugas, S., Gimenez, J., 2010. Degradation of the emerging contaminant ibuprofen in water by photo-Fenton. Water Res. 44, 589–595.

Musa, K.A., Eriksson, L.A., 2007. Theoretical study of ibuprofen phototoxicity. J. Phys. Chem. B 111, 13345–13352.

Nie, G., Huang, J., Hu, Y., Ding, Y.B., Han, X.Y., Tang, H.Q., 2017. Heterogeneous catalytic activation of peroxymonosulfate for efficient degradation of organic pollutants by magnetic Cu^0/Fe_3O_4 submicron composites. Chin. J. Catal. 38, 227–239.

Niu, Y.L., Huang, X.Q., Hu, W.H., 2016. Fe_3C nanoparticle decorated Fe/N doped graphene for efficient oxygen reduction reaction electrocatalysis. J. Power Sources 332, 305–311.

Qin, Y.L., Ding, Y.B., Tang, H.Q., 2016. Highly efficient visible-light photocatalytic activity of graphitic carbon nitride prepared from melamine-thiourea molecular composite. J. Environ. Chem. Eng. 4, 4374–4384.

Rastogi, A., Alabed, S.R., Dionysiou, D.D., 2009. Sulfate radical-based ferrous-peroxymonosulfate oxidative system for PCBs degradation in aqueous and sediment systems. Appl. Catal. B 85, 171–179.

Ren, L., Lu, S.Y., Fang, J.Z., Wu, Y., Chen, D.Z., Huang, L.Y., et al., 2017. Enhanced degradation of organic pollutants using $Bi_{25}FeO_{40}$ microcrystals as an efficient reusable heterogeneous photo-Fenton like catalyst. Catal. Today 281, 656–661.

Shi, P.H., Su, R.J., Wan, F.Z., Zhu, M.C., Li, D.X., Xu, S.H., 2012. Co_3O_4 nanocrystals on graphene oxide as a synergistic catalyst for degradation of Orange II in water by advanced oxidation technology based on sulfate radicals. Appl. Catal. B 123, 265–272.

Stankovich, S., Dikin, D.A., Piner, R.D., Kohlhaas, K.A., Kleinhammes, A., Jia, Y., et al., 2007. Synthesis of graphene-based nanosheets via chemical reduction of exfoliated graphite oxide. Carbon 45, 1558–1565.

Vieno, N.M., Tuhkanen, T., Kronberg, L., 2005. Seasonal variation in the occurrence of pharmaceuticals in effluents from a sewage treatment plant and in the recipient water. Environ. Sci. Technol. 39, 8220–8226.

Wang, N., Zhu, L.H., Wang, D.L., Wang, M.Q., Lin, Z.F., Tang, H. Q., 2010. Sono-assisted preparation of highly-efficient peroxidase-like Fe_3O_4 magnetic nanoparticles for catalytic removal of organic pollutants with H_2O_2. Ultrason. Sonochem. 17, 526–533.

Wang, X.B., Huang, S.S., Zhu, L.L., Tian, X.L., Li, S.H., Tang, H.Q., 2014. Correlation between the adsorption ability and reduction degree of graphene oxide and tuning of adsorption of phenolic compounds. Carbon 69, 101–112.

Wang, X.B., Qin, Y.L., Zhu, L.H., Tang, H.Q., 2015a. Nitrogen-doped reduced graphene oxide as a bifunctional material for removing bisphenols: Synergistic effect between adsorption and catalysis. Environ. Sci. Technol. 49, 6855–6864.

Wang, X.B., Zhang, P., Gao, J.J., Chen, X.D., Yang, H., 2015b. Facile synthesis and magnetic properties of Fe_3C/C nanoparticles via a sol-gel process. Dyes Pigments 112, 305–310.

Wilson, M., 1999. Naproxen and ibuprofen provide the best pain relief for primary dysmenorrhea. Evidence-based Obstet. Gynecol. 1, 108.

Xu, Z.W., Li, H.J., Li, W., Cao, G.X., Zhang, Q.L., Li, K.Z., et al., 2011. Large-scale production of graphene by microwave synthesis and rapid cooling. Chem. Commun. 47, 1166–1168.

Xuan, S., Wang, Y.X., Yu, J.C., Leung, K.C., 2009. Preparation, characterization, and catalytic activity of core/shell Fe_3O_4@ polyaniline@au nanocomposites. Langmuir 25, 11835–11843.

Yang, J.C.E., Yuan, B., Cui, H.J., Wang, S., Fu, M.L., 2017. Modulating oxone-MnO_x/silica catalytic systems towards ibuprofen degradation: Insights into system effects, reaction kinetics and mechanisms. Appl. Catal. B 205, 327–339.

Yao, Y.J., Zhang, J., Wu, G., Wang, S.B., Hu, Y., Su, C., et al., 2017. Iron encapsulated in 3D N-doped carbon nanotube/porous carbon hybrid from waste biomass for enhanced oxidative activity. Environ. Sci. Pollut. Res. 24, 7679–7692.

Yu, L., Chen, J.D., Liang, Z., Xu, W.C., Chen, L.M., Ye, D.Q., 2016. Degradation of phenol using Fe_3O_4-GO nanocomposite as a heterogeneous photo-Fenton catalyst. Sep. Purif. Technol. 171, 80–87.

Zhang, G.Q., Wang, S., Yang, F.L., 2012. Efficient adsorption and combined heterogeneous/homogeneous Fenton oxidation of amaranth using supported nano-FeOOH as cathodic catalysts. J. Phys. Chem. C 116, 3623–3634.

Zhang, T., Zhu, H.B., Croué, J.P., 2013. Production of sulfate radical from peroxymonosulfate induced by a magnetically separable $CuFe_2O_4$ spinel in water: efficiency, stability, and mechanism. Environ. Sci. Technol. 47, 2784–2791.

Zhao, Y., Nakamura, R., Kamiya, K., Nakanishi, S., Hashimoto, K., 2013. Nitrogen-doped carbon nanomaterials as non-metal electrocatalysts for water oxidation. Nat. Commun. 4, 2390.

Zhou, Y., Jiang, J., Gao, Y., Ma, J., Pang, S.Y., Li, J., et al., 2015. Activation of peroxymonosulfate by benzoquinone: a novel nonradical oxidation process. Environ. Sci. Technol. 49, 12941–12950.